Turkish Journal of Physics

http://journals.tubitak.gov.tr/physics/

Invited Review Article

Turk J Phys
(2014) 38: 543 – 562

doi:10.3906/fiz-1407-1

Electron field emission from nanostructured semiconductors under photo illumination

Oktay YILMAZOGLU[1,*], Anatoli EVTUKH[2], Shihab AL-DAFFAIE[1], Jens-Peter BIETHAN[1], Dimitris PAVLIDIS[3], Vladimir LITOVCHENKO[2], Hans L. HARTNAGEL[1]

[1]Technische Universität Darmstadt, Darmstadt, Germany
[2]Institute of Semiconductor Physics, NASU, Kiev, Ukraine
[3]Department of Electrical and Computer Engineering, Boston University, Boston, USA

Received: 01.07.2014 • **Accepted:** 08.10.2014 • **Published Online:** 10.11.2014 • **Printed:** 28.11.2014

Abstract: New device concepts and materials for the fabrication of compact high-frequency vacuum sources and micro-nano-integrated X-ray sources are of particular interest for broadband communication, security screening of packages and chemical materials, biomedical examination, and other applications. This article integrates results on GaN- and ZnO-based nano and self-assembled structures. They were used as field emitter tips for cold electron emission at high local electric fields as well as for photoassisted field emitters to generate bunched electrons directly from the emitter tip. The results on functional field emitters as cold electron sources will be presented. They are key elements for building, among other miniaturized vacuum tubes. Such miniaturized vacuum tubes can achieve high power at high cutoff frequencies and overcome the limitations of conventional GaAs- or InP-based solid-state devices. Furthermore, new functional X-ray sources with ultrashort pulses will allow 3D imaging with low radiation doses.

Key words: Electron field emission, nanorod, GaN, ZnO, photoassisted field emission, electric field enhancement

1. Introduction

Future generations of electronics and sensors will rely more and more on the special features and inherent properties of new devices as the improvement in performance due to progress in design and processing for solid-state devices reaches saturation. Over the last 2 decades, tremendous advances have been made in devices ranging from the introduction of new operation concepts to new material choices and improvement in fabrication processes. Examples of them are devices such as high-electron mobility transistors (HEMTs) with f_{max} = 1.2 THz [1] and heterojunction bipolar transistors (HBTs) instead of the more traditional MESFETs and bipolar junction transistors (BJTs), and InP-, Sb-, III-nitride-, SiGe-based materials instead of Si and GaAs. Processing has also improved, opening the way to submicron devices and pushing the limits of silicon technology to 22-nm node while introducing high-k dielectrics to overcome the difficulties caused by tunneling through ultrathin gates and maintaining good electrical performance. Technological improvements have almost reached their limits and new generations of devices are necessary to enable further advances for high frequency generation. New achievements in high frequency sources have not only practical significance in the scientific context but also beyond, in fields such as pharmacy, chemical recognition for environmental protection, biomedical engineering, remote radar-type sensing, and tomography. Materials analysis, package monitoring, and security screening for

*Correspondence: yilmazoglu@hfe.tu-darmstadt.de

civil defense are other possible applications [2] (Picometrix LLC, Ann Arbor, MI, USA). It has also become clear that these systems must be compact, inexpensive, and easy-to-use to permit development into a technology of interest for broader markets outside of science. The majority of application requires in general the availability of inexpensive and moderate technology with room-temperature application.

New electronic devices are currently intensively studied in view of developing new solid-state components [3]. Wide bandgap semiconductors, such as GaN, ZnO, and SiC, are very promising for novel applications up to THz frequencies, and are very suitable for high power, high-temperature, and harsh environment operation [4–7] due to the high saturation velocity, high breakdown voltage, and direct bandgap.

Semiconductor materials based on group-III nitrides have acquired immense importance worldwide, mainly because of their large electronic bandgap. This allowed closing significant gaps in the fabrication of short wavelength optoelectronic devices as blue, green, and UV LEDs; UV and blue laser diodes; and short-wave detectors [8,9]. The large bandgap and the chemical and thermal stability allow the application in high power, high frequency electronics [4]. An improvement in microwave power density by about an order of magnitude compared to the GaAs material system was demonstrated [10]. Important also are the positive characteristics such as high saturation drift velocity of electrons of nearly 3×10^7 cm/s [11] and extremely high breakdown field strengths of 3–5 $\times$ 10^6 V/cm [9,12]. Efficient components up to the terahertz region can be developed with nitride heterostructures [5,6,13] due to their high energy barriers, high breakdown fields, and larger saturation drift velocities. Furthermore, these materials find application for various sensor concepts because of their large piezoelectric coefficients and robustness in harsh environments.

Novel cold electron emitters (field emitters) fabricated with the help of nano and self-assembled structures can help to overcome the frequency and power limitations [14,15] of high frequency devices and have versatile applications in measurement and sensor technology (e.g., scanning electron microscopy and X-ray image sensors) [16,17]. The temperature and radiation resistance of field-emitter components are of particular interest for the fabrication of efficient and robust microwave sources (triode, miniaturized vacuum tube amplifiers).

With the availability of modern micro-nano-fabrication techniques, it became possible to fabricate vacuum nanoelectronic components based on field emitters (cold emitters), which are suitable for the high frequency region. The required field strengths for field emission can be achieved by nano and self-assembled structures (semiconducting) field emitter tips (radius $\sim$ 10 nm and field enhancement factor $>$ 1000). In such devices, electron transport is performed through a vacuum without scattering, as is in case of solid-state components, setting up therefore the basis for attaining ultrahigh frequency operation. Efficient electron field emission cathodes are of major importance. New developments in field emitter arrays (FEAs) with nanoemitters are therefore discussed and experimentally investigated. FEAs with high current densities are considered promising sources of cold electrons in miniature tubes for millimeter-wave generation as well as new X-ray sources with ultrashort pulses and low radiation doses.

2. Functional field emitter

The above-mentioned unique applications of new vacuum devices have initiated intensive studies in the area of field emission of cold cathode materials. Field emitters with a small emitter tip radius and long arrays (e.g., carbon nanotubes, semiconductor nanowires) are necessary for high field enhancement factors and thus low operating voltages. The electric field enhancement β on the tip of the field emitting cathode can be presented in the approximation of a floating sphere as $\beta \approx h/r + 3$ [18], where h and r are the tip height and radius of curvature, respectively.

Furthermore, small operating voltages can be achieved with a small emitter-gate spacing (realized with an easily integrated gate) or materials with small work function (e.g., GaN, AlGaN, AlN, diamond, and diamond-like carbon (DLC)) [19–24]. In the case of wide bandgap materials with low electron affinity an important issue for field emission is the electron transport to the surface. Besides low work function (electron affinity) it is essential to have (i) good electron injection on the back contact, and (ii) easy electron transport through the emitter material [25]. Therefore, for studies of electron field emission from GaN, AlGaN, and AlN great attention is paid to ultrathin and highly doped films [24,26,27]. Important for large-scale production is the use of materials that are easy to process, in order to achieve structures with high field enhancement factors, and have a good chemical stability, high mechanical strength, and high thermal conductivity.

Field emission itself is a quantum mechanical tunneling effect (named cold emission) and starts at electric fields F $> 10^7$ V/cm. The energy band structure of a metallic emitter at field emission is shown in Figure 1. The field emission current density J (A/cm^2) depends exponentially on the work function of the emitting surface Φ (eV) and the local electric field F (V/cm) just above the emitter surface. The well-known Fowler–Nordheim (FN) equation can be written as:

$$J = A\frac{F^2}{\Phi}\exp(-B\frac{\Phi^{3/2}}{F}), \tag{1}$$

where A and B are constants given by A $= 1.54 \times 10^{-6}$ AeVV^{-2} and B $= 6.83 \times 10^7$ (eV)$^{-3/2}$ Vcm^{-1}. If the distance between cathode and anode is d, then the field enhancement factor β is defined by F $= \beta$V/d $= \beta$E, where V is the applied voltage across the device electrodes and E the macroscopic electric field.

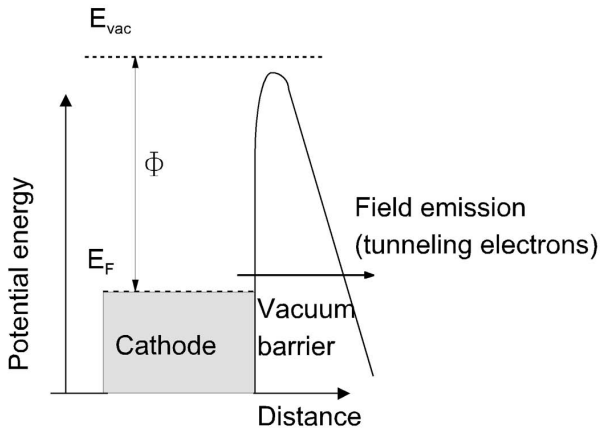

Figure 1. Energy band structure with bending of the vacuum barrier at field emission.

Various field emitter materials have been intensively studied. Semiconductor materials such as GaAs, GaN, AlGaN, and ZnO, as well as carbon-based ones (e.g., carbon nanotube) have been used to explore the fundamental properties of the semiconductors themselves, as well as their field-emission properties. The field emitters have been nanostructured by various techniques such as photoelectrochemical (PEC) etching [7] but self-assembled nanorods [28] or nanotubes have also been used for these studies. The use of low dimensional wide bandgap structures provides the possibility of nano-engineered bandstructures (growth of the energy gap, decreasing of the energy distance between main and satellite valleys in the conduction band, etc.) caused by quantum-size confinement effect upon decreasing of the geometrical sizes to nanometer scale [20]. Hereby one can control the transport and emission properties. The energy band diagram of GaN has, similar to

GaAs, 2 subbands for light and heavy electrons in the conduction band [7,29] (Figure 2a). Further investigated materials such as AlGaN and ZnO have also similar conduction band schemes with different values of the energy difference between the Γ and the satellite valley. A method based on field emission under photo illumination was reported that allows one to determine the values of the energy difference between the Γ and the satellite valley in the conduction band [20]. Field emitters based on novel semiconductor wide bandgap materials (such as GaAs, GaN, AlGaN, and ZnO) have been characterized with and without (laser) light illumination, where modified emission properties were obtained. These have very small threshold field strengths and stable emission currents. The measurements were used to characterize multiple valley energy-bands and show the possibility of laser-modulated electron emission to obtain bunched electrons directly from the emitter tip.

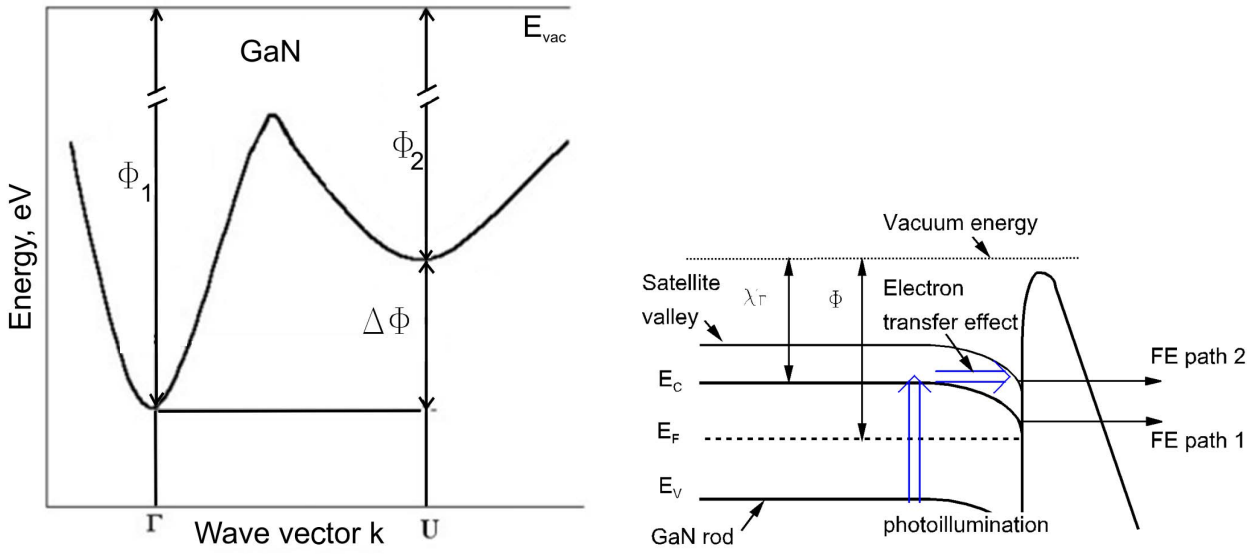

(a) (b)

Figure 2. (a) Conduction band diagram of GaN with 2 valley positions. (b) Energy band diagram of GaN with emission from GaN Γ-valley (path 1) and from GaN satellite valley (path 2).

A conventional traveling wave tube with a molybdenum field emitter (Spindt emitter) as cathode was fabricated and investigated [30] (Figures 3 and 4a). A current density of J = 15.4 A/cm^2, absolute current of I = 121 mA, output power of P = 100 W, and operation frequency of f = 5 GHz was obtained for a tube length of L = 16 cm.

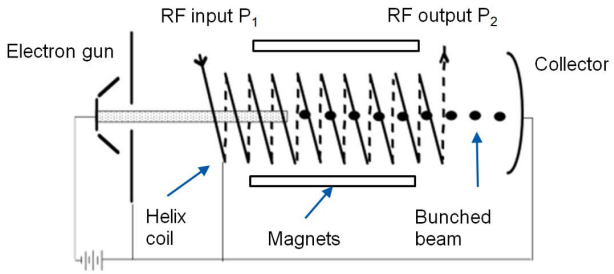

Figure 3. Traveling wave tube with cold electron emitter as cathode [30].

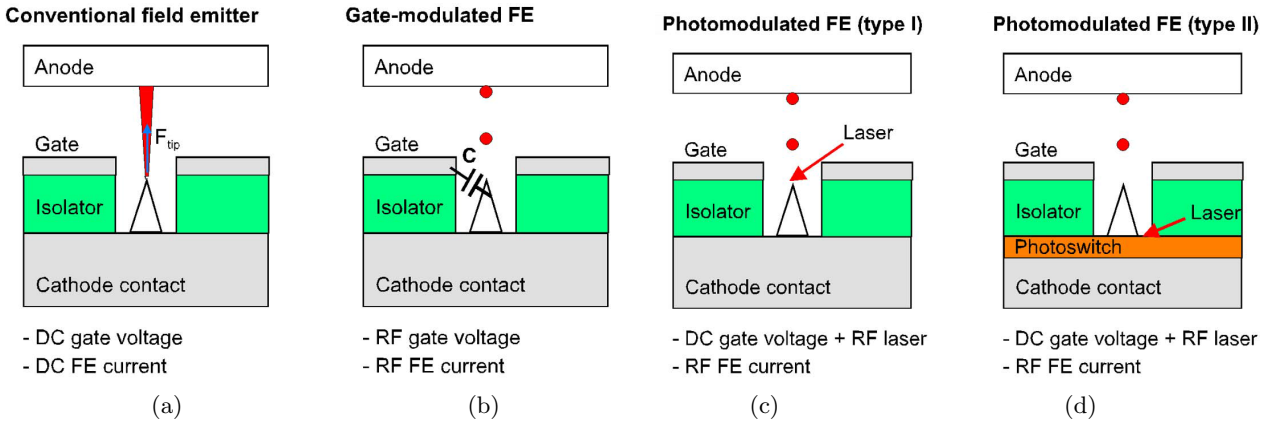

Figure 4. Conventional (a) and functional (b–d) field emitters.

New functional field emitters with bunched electrons can be used for miniaturized vacuum devices. They open the possibility for density modulation of the electron beam with a gate electrode (Figure 4b) or photomodulation (Figure 4c) instead of velocity modulation (Figure 3) after electron emission in the vacuum tube. A new device made of a combination of a carbon-based emitter with low threshold field and ultrafast compound semiconductor photoswitch (e.g., low-temperature grown GaAs) was also used for modulated electron emission (Figure 4d). This new electron source with ultrashort electron bunches will allow a greater range of applications.

The advantages obtained by pre-bunching the beam are high efficiency and a significant reduction in the required RF interaction length in the tube, thereby simplifying beam transport magnetics and reducing the weight. Devices with high power and high efficiency can be obtained [31,32]. Furthermore, laser or LED modulated field-emitters can generate ultrashort electron bunches for pulsed X-ray sources [33,34] or even for THz and X-ray free electron lasers (FELs) [35–37]. The production of short electron bunches with lower emittance and higher brightness than the state-of-the-art would have consequences in a variety of scientific and industrial applications. It is the most direct way to reduce the cost and size of free electron lasers.

A field emission set-up was put in place based on such approaches for analyzing the material properties of semiconducting emitters as GaN, AlGaN, and ZnO. A (photoassisted) field emission spectroscopy method was developed for characterization of the energy bands of wide bandgap materials used in solid-state and vacuum nanoelectronic devices. Their potential for high frequency generation was also evaluated.

3. Self-arranged wide bandgap semiconducting field emitters (GaN, AlGaN, and ZnO)

The work described in this section reports a simple fabrication of ordered field emitter tips with the help of self-arranged nano-structures. Stable field emitter structures have already been demonstrated using a sophisticated etching technology in InAs materials [38]. The resulting surface consisted of high density nanostructures with cone shapes. GaN-based materials are very promising for field emitters. GaN has superior properties such as a low electron affinity of $\sim$3.4 eV [21], mechanical hardness, and chemical inertness. Photoelectrochemically etched GaN is often not homogeneous over large areas. However, using smaller pre-defined n^+-GaN mesas, an improved homogeneity of one-dimensional nanowires in these areas was achieved [7]. These emitter arrays could stabilize the field emission due to the presence of redundant emitters and averaging of the current instabilities of single emitters.

GaN is a compound semiconductor with multiple valleys in the conduction bands (see Figure 2a). The

energy separation of the valleys is much higher than in other materials, e.g., GaAs. Such a particular band structure can be used for modulated electron field emission by filling the upper valley with electrons. The vacuum energy barriers for electron field emission from main and satellite valleys are different (see Figure 2a). In spite of the low energy barrier of the upper valley, its impact on the emission current can be remarkable after hot electron filling due to the Gunn (electron transfer) effect. The use of additional light illumination of such electron field emitters allows the electron transfer effect to be sustained and decreases the effective work function [7,39–41]. Photoassisted field emitters are perspective as modulated electron emitters for application in vacuum micro- and nanoelectronics. An important requirement for such applications is the use of materials with ultrafast relaxation time from the satellite valley. These devices can overcome the frequency limitations of grid controlled cathodes. The photoassisted field emitter is not limited by the cathode-grid input capacitance and introduces an alternative mean of bunched beam production limited only by the cut-off frequency of Gunn diodes based on these materials.

Although considerable work has been reported on the experimental investigations of GaN devices, much less has been published on their bandstructure and material characteristics. This applies in particular to nanostructured materials like nanowires and nanodots, where new effects were predicted [42–44].

The energy separation between the valleys can be calculated from field emission measurements. The possibility of investigating the electron states between the Fermi and vacuum levels by studying the field emission of optically excited electrons has been discussed previously [45,46]. This method is based on the work function changing under photoexcitation of electrons or hot electrons at their tunneling through a barrier according to the FN mechanism. A (photoassisted) field emission spectroscopy method was developed for characterization of the conduction band structure of wide bandgap materials such as GaN, AlGaN, and ZnO [7,20,28,29,38–40,47–50]. It is based on pure field emission or employs light emitting diodes (LEDs) or an optical laser for photoexcitation of electrons. It can be applied for material characterization used in solid-state and vacuum nanoelectronic devices. Wide bandgap materials were investigated using this technique and their potential for high frequency generation was evaluated. The knowledge of the exact band structure of e.g. GaN is essential for optimal device design and function, and was very helpful in the preparation and characterization of the GaN Gunn diodes [5,6,51–53]. The electron transfer effect (Gunn effect) could also be shown for AlGaN and ZnO materials. Experimental results for the electron transfer effect in these materials are very limited or nonexistent. The described spectroscopy method could be further used for the estimation of the energy band reconstruction due to quantum confinement effects in nanostructured semiconductor surfaces.

3.1. Fabrication

3.1.1. Fabrication of nanostructured GaN

The GaN field emitter rods were fabricated by top-down approaches such as PEC etching on a GaN substrate. The wafer had an n-GaN active layer of 5 μm sandwiched between an n^+-GaN cap layer of 100 nm and a 300-μm-thick n^+-GaN substrate. The active layer and the top n^+-GaN layers were grown by metal organic chemical vapor deposition with trimethylgallium (TMGa) and ammonia (NH_3) as source materials. A photoresist mask served for argon plasma etching (Ar flow of 20 SCCM, background pressure of 50 mTorr, and rf power of 300 W) of a circular mesa 400 nm in height. First, the n^+-GaN layer was etched in the area surrounding the mesa. The n-GaN layer cap uncovered as a result of this process was not affected at this step [7]. The samples were then cleaned in acetone and etched by PEC etching. UV illumination generates electron-hole pairs at the n^+-GaN surface, which enhance the oxidation and reduction reactions taking place in the electrochemical cell, formed

by immersing the substrate in a 0.1 M KOH stirred solution. This allows one to achieve selectivity in etching n^+-GaN with respect to n-GaN [7]. The GaN sample was PEC etched for 12 min in the presence of Hg lamp illumination.

The GaN field emitter rods resulting from this processing are shown in Figure 5. Further etching up to 38 min increased the height of the rods by extending them into the n-GaN layer below the n^+ cap. The n-GaN material around the mesa was not affected by this step and remained unetched (see Figure 5a). The selectivity in etching the area containing the nanorods but not the surrounding area is due to the presence of the thin n^+-GaN layer in the mesa area, which promotes PEC etching. GaN rods are promising field emitter structures due to their small tip radii, which lead to electric field enhancement and reduced effective electron affinity. The formation of high quality GaN NWs with controllable diameter and length, and uniform distribution is a challenging task and required extensive experimental studies.

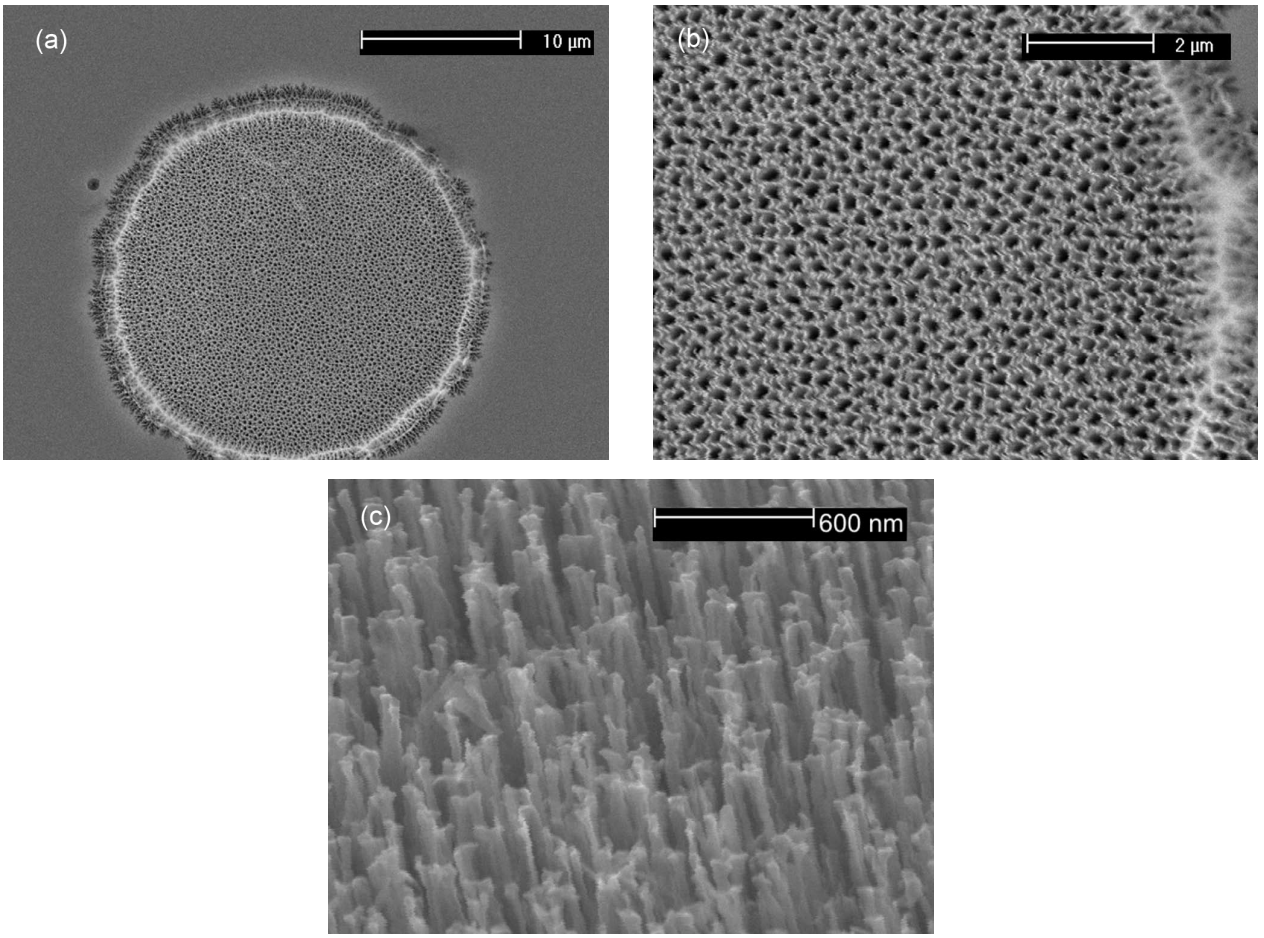

Figure 5. GaN nanowires produced by PEC etching. They are well aligned and have small tip radii for efficient field emission. SEM images with higher magnification are shown in (b, c).

Some etched GaN surfaces showed extremely small nanomorphologies (see Figure 6a). Such quantum-size dimensions can increase the energy bandgap and thus reduce the effective work function as given in Figure 6b.

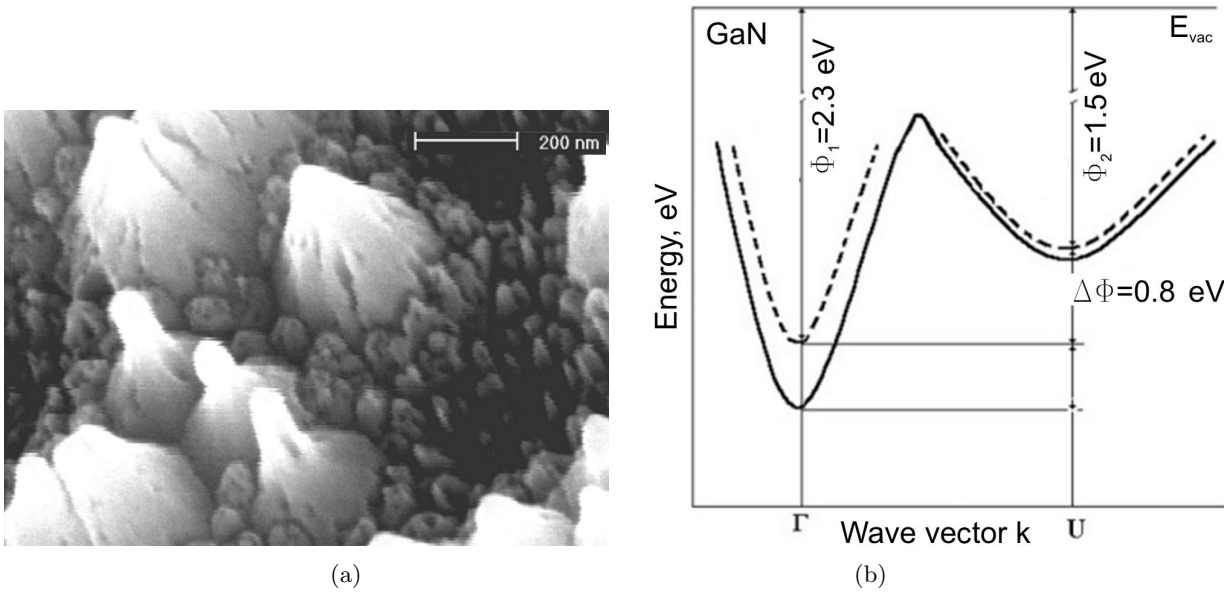

(a) (b)

Figure 6. (a) GaN surface nanomorphology and (b) energy shift of valley positions due to the quantum-size restriction effect in GaN nanostructures.

3.1.1.1 Selective growth of GaN

GaN-based field emitters were fabricated by selective growth of n-GaN on GaN/sapphire layers using a 1-μm-thick SiN_x mask (see Figure 7). The study aimed at emitters with a small tip diameter. Circular openings with various diameter sizes were patterned in the SiN_x mask by reactive ion etching. The growth rate and homogeneity in the openings were found to depend on the effective area opening, gas flow, gas modulation, and substrate temperature. Lateral overgrowth on the 1-μm-thick SiNx mask was possible by means of a growth condition. The surface flatness and lateral overgrowth were studied by optical and scanning electron microscopy [54].

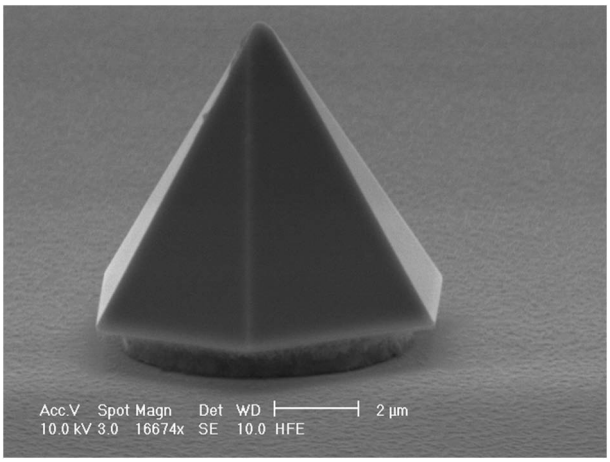

Figure 7. SEM image of a hexagonal pyramid on the patterned substrate.

3.1.2. Fabrication of nanostructured AlGaN

The AlGaN structure used in our experiments was grown by low-pressure MOCVD on (0001) c-plane sapphire. A buffer layer of about 25-nm-thick GaN was first grown at 510 °C on sapphire. The investigated multilayer structures had AlGaN upper layers on GaN. A patterned Ti mask served as electrical contact to the sample as well as etch mask. The Ti metal contacts were unannealed. Quantum dots were formed by PEC etching of GaN [55]. Under high current conditions and under process-specific conditions it led in high etch selectivity at the dislocations. PEC etching of GaN is a means of greatly improving the chemical reactivity of GaN at room temperature. Ultraviolet illumination generates also here electron–hole pairs at the semiconductor surface, which enhance the oxidation and reduction reactions within an electrochemical cell. The GaN and AlGaN were etched from 1 to 15 min in a stirred 0.1 M KOH solution using Hg lamp illumination. The schematic cross-section of nanometer-size tips is shown in Figure 8.

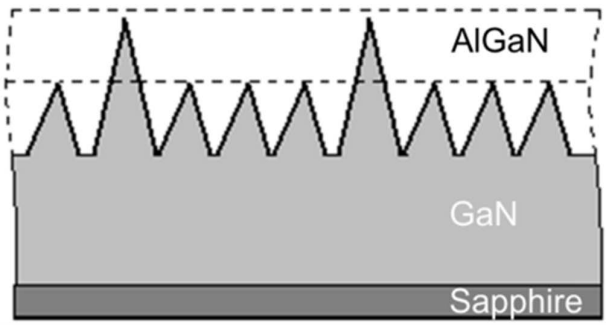

Figure 8. Schematic of the nanostructured AlGaN/GaN heterojunction surface.

3.1.3. Fabrication of nanostructured ZnO

The energy band diagram of ZnO is also of interest for use in ZnO-based devices. So far the majority of the device results published in the case of ZnO-based nanostructures [56,57] are based on randomly ordered NWs. Thus, ZnO field-emitter whiskers with nanometer diameter were fabricated by metal-organic chemical vapor deposition (MOCVD) growth on Si substrates (see Figure 9) [28,58,59]. These ZnO field-emitter whiskers have vertically ordered conical nanometer structures and were grown catalyst-free by MOCVD on (100)-Si substrates (Figure 9). To achieve good crystal quality and to address the issue of difference in crystal structure between the grown layers and the substrate, a low temperature nucleation buffer layer was first deposited on the silicon surface at low temperature ∼340 °C. The precursors were oxygen and diethylzinc (DEZ) (bath temperature 30 °C), while the carrier gas was nitrogen. The reactor pressure was controlled to be 20 mbar. The DEZ carrier gas and oxygen flow were 75 sccm and 25 sccm, respectively. The high temperature growth steps took place at 500 °C where the oxygen and DEZ flow were 100 sccm each. The layer features were monitored using a homemade in situ laser interferometer [28,58]. A typical nucleation layer involves a 2-stage growth process where island formation results in reduction of reflectivity, followed by growth of either flat top areas covering the islands or of a planar layer leading to the start of an oscillation. The density and the size of the obtained ZnO nanowires are dependent on the growth conditions and can therefore be controlled. The resulting ZnO tips had nanometer size, which is important for high field enhancement and simpler electron emission at smaller bias voltages (Figure 9). A detailed study of the interferometry of ZnO MOCVD growth and its relevance to nanostructure growth is given by Biethan et al. [58].

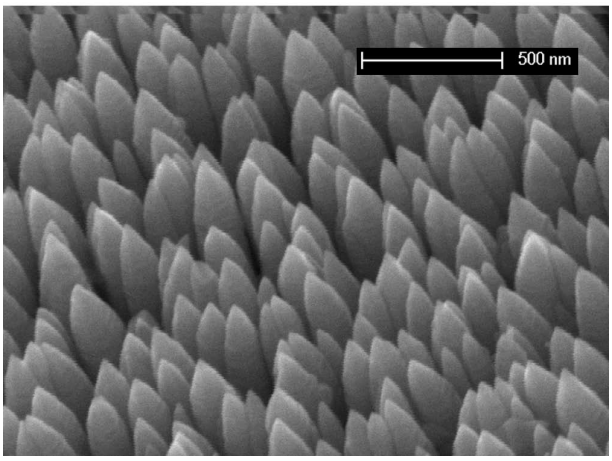

Figure 9. ZnO nanowires produced by process specific MOCVD growth. They are well aligned and have small tip radii for efficient field emission.

3.2. Field-emission measurements

The field emission properties of all nitride-based and ZnO samples were measured using a parallel plate configuration at room temperature in a vacuum chamber evacuated to the pressure of $\sim 5 \times 10^{-8}$ mbar. The bottom sides of the field emitter samples were fixed to a metal electrode using a conducting carbon pad or silver paste to form a cathode contact. A heavily doped Si wafer was used as an anode electrode with a defined emitter–anode distance (Figure 10a). For the measurement with photo illumination a light transparent indium tin oxide coated quartz glass was used instead of the former Si anode [7]. A UV LED ($\lambda \sim 365$ nm, $P_{opt} = 100$ mW) was connected to the anode side for illuminating the sample during field emission measurements. The field emitter was placed in the high vacuum chamber and the LED beam was focused directly on it through the quartz glass (Figure 10b).

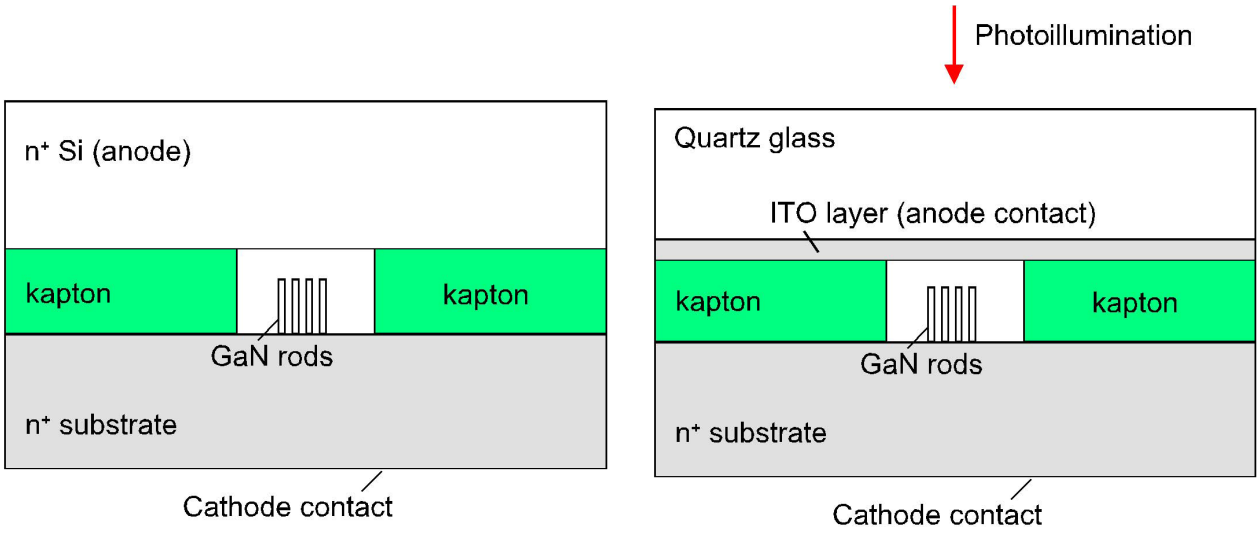

Figure 10. Biasing scheme of the GaN rod field emitter (a) without and (b) with UV LED photoexcitation in the vacuum chamber.

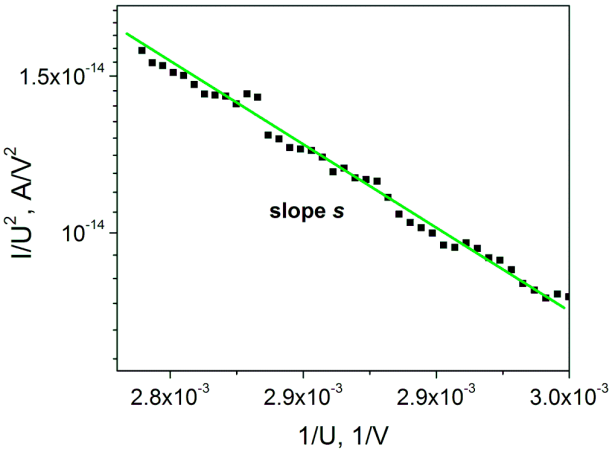

(c)

Figure 10. (c) Fowler–Nordheim characteristics of a field emitter without illumination.

The distance between the emitter and external anode was controlled by a kapton spacer disk (e.g., thickness 7.5 μm and diameter 1 mm). The LABVIEW program was then employed to measure the I-V characteristics. The dependencies of the field emission current density on the applied electric field and the corresponding FN plots [log(I/U^2) vs. 1/U] without (Figure 10c) and with photoillumination were measured.

The straight line in the FN characteristics in Figure 10c evidences field emission of electrons through the potential barrier into the vacuum (see Figure 1).

The field enhancement factor can be calculated from the initial slope s of the FN plot [log(I/U^2) vs. 1/U] using the following equation:

$$\beta = -2.84 \times 10^7 (d_{EA}\ \Phi^{3/2})/s, \tag{2}$$

where d $_{EA}$ is the emitter–anode distance in cm, Φ is the work function of the emitter in eV (e.g., $\Phi_{GaN} = 3.3$ eV), and β is the field enhancement factor.

3.2.1. Field emission of GaN nanorods

The photoelectrochemically etched GaN whisker structures have a small tip diameter of 10–50 nm with high electric field enhancement and reduced turn-on fields down to E = 4 V/μm [7,60]. These nanoemitters produced a maximum current density of about J = 40 mA/cm^2. Excellent field emission characteristics were also demonstrated from GaN nanorods of 50 nm average diameter grown on silicon [61]. Their field emission turn-on was as low as 1.25 V/μm at a current density of 0.1 μA/cm^2 and a field emission current density as high as 2.5 mA/cm^2 at an applied field of 2.5 V/μm [61].

The energy band diagram of GaN is similar to that of GaAs having 2 subbands for light and heavy electrons in the conduction band (see Figure 2a). An important difference of the wide bandgap semiconductors compared with traditional III–V compounds is their large intervalley distance (1–2 eV or higher). Many groups have theoretically calculated the bandstructure for GaN [62,63] and measured some of its characteristic values, i.e. the intervalley energy difference [20,64–66]. UV photoelectron spectroscopy allows one to determine the electron affinity of III-nitrides and their alloys. However, the measured values of the energy difference between the Γ-valley and the satellite valley differ from the calculated ones.

3.2.1.1 Field-emission spectroscopy in GaN materials

A new method was developed [7] for estimating the conduction band characteristics based on field emission measurements under UV illumination. It requires evaluation of the field emission current from the lower and upper conduction subbands of the semiconductor and is useful for evaluating wide bandgap materials such as GaN and ZnO and their alloys. The linear FN characteristic showed a change in the slope for emission from different subbands (see Figure 11), which depends on the specific affinities of the emitted electrons (Figure 2 and formula 3 where β was constant for both valleys [7]). Wide bandgap materials present much more favorable conditions for the field emission spectroscopy compared to GaAs, which has a small subband energy difference (ΔE) value of 0.31 eV.

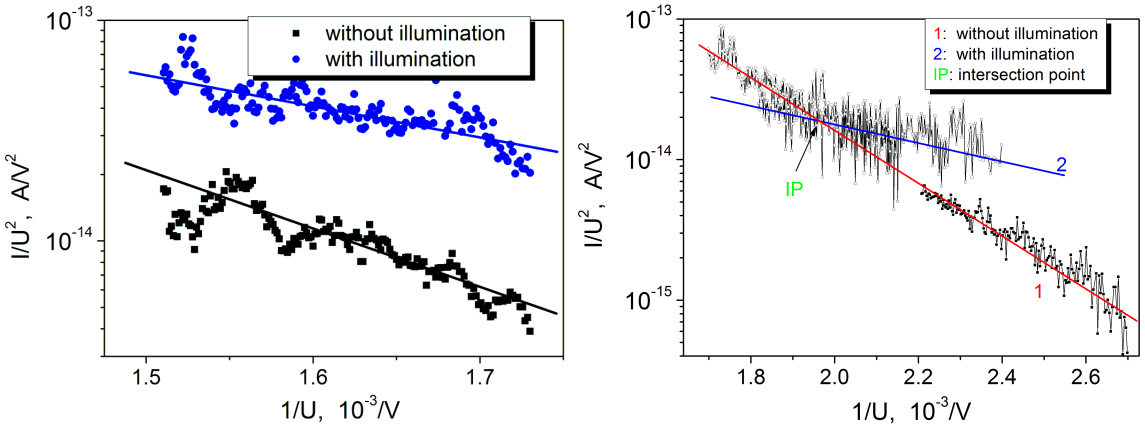

Figure 11. Fowler–Nordheim characteristics of GaN emitters with and without UV LED illumination for 2 different samples (a, b).

Upon UV LED illumination, the current increased immediately, and was up to one order of magnitude higher than the initial current. Illumination results in electron-hole pair generation by absorption of UV photons with energies larger than the bandgap of the GaN nanorods, 3.4 eV. Electrons can then reach the surface quickly due to the small diameter of the GaN nanorods. The field necessary for field emission penetrates into the depleted GaN rod (electrical field $E > E_{th} = 150$ kV/cm) and enables electron transfer from the Γ-valley to the satellite valleys. The photoexcited electrons can then contribute to the field emission process from the satellite valley due to their smaller electron affinity χ (see Figure 2b, path 2). The electron field emission current shown in the FN plot (Figure 11) clearly demonstrates 2 different slopes for nonilluminated and UV illuminated emission.

In the case where the GaN rods are not illuminated, the emitter is almost depleted and emission takes place from the Γ-valley $\chi_{GaN} = 3.3$ eV. Upon UV illumination, new electrons are generated from the valence band and occupy the upper valley. The main emission occurs from this valley, which has lower electron affinity. The presence of a high electric field in the emitter tip supports the presence of the electron transfer effect. The field emission current from the satellite valley increases rapidly and becomes dominant at a rather small electron concentration n in the upper valley due to the much smaller electron affinity in this valley, as compared with the Γ-valley (see transition from slope 1 to slope 2 in Figure 11b). Increasing the electric field strength reduces the vacuum barrier thickness, and increases the tunneling probability and the contribution from the main valley due to the larger number of electrons. The total field emission current is dominated again by the main valley emission at electrical field strengths above the interception point IP (see Figure 11b).

The effective work function (electron affinity) can also be calculated by considering the slope s of the FN characteristic [$\log(I/U^2)$ vs. $1/U$]:

$$s = -2.84 \times 10^7 \times d_{EA} \times \Phi_{eff}^{3/2} = -2.84 \times 10^7 \times d_{EA} \times \Phi^{3/2}/\beta \quad (3)$$

with

$$\Phi_{eff} = \frac{\Phi}{\beta^{2/3}},$$

where d_{EA} is the emitter-anode distance in cm, Φ is the real work function of the material in eV, and β is the electric field enhancement coefficient due to the geometry of the emitter. In practice it is difficult to estimate the field enhancement coefficient β to separate the influence of the real work function Φ and β on the determined effective work function. However, a first estimation can be made by analyzing the surface morphology from SEM pictures [18]:

$$\beta \approx \frac{h}{r} + 3,$$

where h is the tip height and r is the curvature radius of the top.

It is also possible to determine the ratio of Φ_1/Φ_2 (work function for Γ-valley/work function for the satellite valley) and the electron affinity difference (equal to the energy difference between the valleys; see Figure 2) from the 2 slopes in FN plots assuming that β is constant (Figure 11a):

$$\Phi_1/\Phi_2 = \chi_\Gamma/\chi_{Satellite} = (s_1/s_2)^{2/3}$$

The obtained value of $\chi_\Gamma/\chi_{Satellite} = 1.53$ (GaN rod) can be used to calculate $\chi_{Satellite}$ for given values of χ_Γ, i.e. $\chi_\Gamma = 3.3$ eV. The calculated $\Delta E = 1.15$ eV from the FN characteristics is in good agreement with values reported previously [65] ($\Delta E = 1.1$ eV).

The band structure reported above can be used for modulated electron field emission and applied to the realization of high frequency sources in miniaturized vacuum micro- and nanoelectronics as well as for bunched electron generation for pulsed X-ray sources. The evaluation of the position of the first upper valley in GaN rods is also an important issue for better understanding of devices such as Gunn diodes made with such materials. A detailed spectroscopy study of the GaN bandstructure with different valleys can be possible by field emission measurements using tunable monochromatic illumination of the emitter tips.

The slope change in the case of emission from GaN nanostructured surfaces is also good evidence for the quantum confinement effect on nanosized cathodes. Some nanostructured surfaces of GaN had nanometric tip diameter ($d < 10$ nm; lower emitter in Figure 6a). Under such circumstances, the quantum-size confinement effect causes an energy band reconstruction (Figure 6b). The energy bandgap was increased and the free carrier concentration in the Γ-valley was decreased, which negatively influences the field emission. However, the electron affinity was also decreased, which positively influences the field emission. It was also shown for GaN [20,29] that the energy difference between the $\Gamma-$ and X-valley was decreased to 0.8 eV (Figure 6b), thus increasing the probability of electron transition from $\Gamma-$ to $X-$valley at the same electric field. The experimental FN characteristic (Figure 12, curve 1) was compared with simulated FN characteristics of different band structures with intervalley distance of 0.5 eV (curve 2), 0.7 eV (curve 3), and 0.8 eV (curve 4). The theoretical and experimental curves are practically coincident for $\Delta E = 0.8$ eV (Figure 12, curves 1 and 4). The sharp current increase at low electric fields for a small intervalley distance in GaN (Figure 12, curve 2 with $\Delta E = 0.5$ eV) was caused by easier intervalley carrier redistribution and the low work function of the quantum-sized cathode.

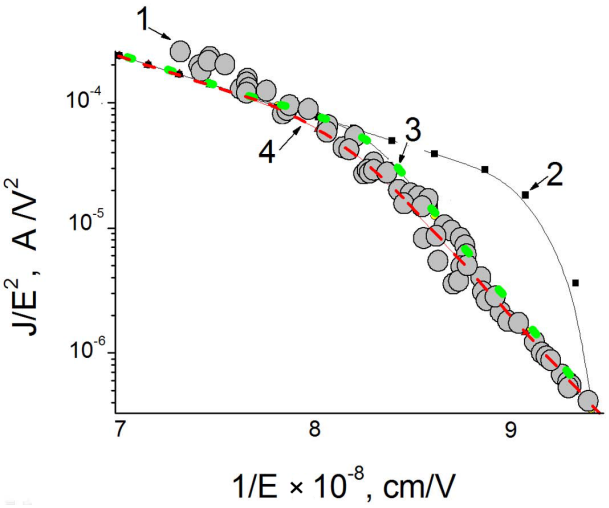

Figure 12. Fowler–Nordheim characteristics of the quantized GaN structures. Measurement (curve 1) and simulations with intervalley distance of 0.5 eV (curve 2), 0.7 eV (curve 3), and 0.8 eV (curve 4).

Further optimization of the spectroscopy technique was performed [67]. The presence of the image force and vacuum barrier height correction was taken into account. Furthermore, the influence of band bending and Fermi level shifting due to high electric field penetration was introduced, and showed only a small correction factor.

3.2.2. Field emission of AlGaN nanoemitters

AlGaN/GaN heterostructure field emitters have been investigated as an alternative to bulk designs. The work function of the proposed GaN nanorod-based field emitter structures can be decreased relatively easily with the help of a GaN-$Al_xGa_{1-x}N$ heterostructure emitter, due to the relatively low electron affinity of AlGaN; the electron affinity of GaN and AlN is 3.3 eV and zero or even negative, respectively. By changing the composition x in the GaN-$Al_xGa_{1-x}N$ structure it is possible to decrease the effective electron affinity and the work function at electron field emission.

The satellite valleys of AlGaN also offer interesting properties for field emission. Good electron injection on the back contact and easy electron transport through the emitter material are essential for this material system. The peculiarities of electron field emission from nanostructured surfaces of AlGaN on GaN were investigated. The surface of the upper layers was nanostructured by PEC etching in water solution of KOH [48]. The change in the FN plots' slope (Figure 13) was used to calculate the effective work functions upon electron field emission.

It is possible to determine the ratio of Φ_{eff1}/Φ_{eff2} for the right two parts (A and B) of the emission curve in FN coordinates:

$$\Phi_{eff\,1}/\Phi_{eff\,2} = \Phi_1/\Phi_2 = \chi_\Gamma/\chi_X = (s_1/s_2)^{2/3},$$

where Φ_{eff} is the effective work function, Φ is the real material work function, and χ is the electron affinity. The experimentally obtained value of $\chi_\Gamma/\chi_X = 1.71$ (AlGaN) can be used with $\chi_{\Gamma,\ AlGaN} = 2$ eV [21] to calculate the electron affinity from the satellite valley as χ_X(AlGaN) = 1.17 eV.

At low electric fields, electrons tunnel directly from the Γ-valley of the bottom GaN layer to the Γ-valley of the upper AlGaN layer, then go through the AlGaN layer and tunnel into vacuum (Figure 14a, path 1). At higher electric fields an electron transfer from the Γ-valley of GaN to the X-valley of AlGaN is possible (Figure

14b, path 2). The probability of indirect tunneling is, however, lower than the direct process due to the need of pulse scattering by phonons or impurity centers. In the case of electron transition from the Γ-valley of GaN to the X-valley of AlGaN the slope of the FN plot is decreased due to lower electron affinity χ_X in the satellite valley of AlGaN.

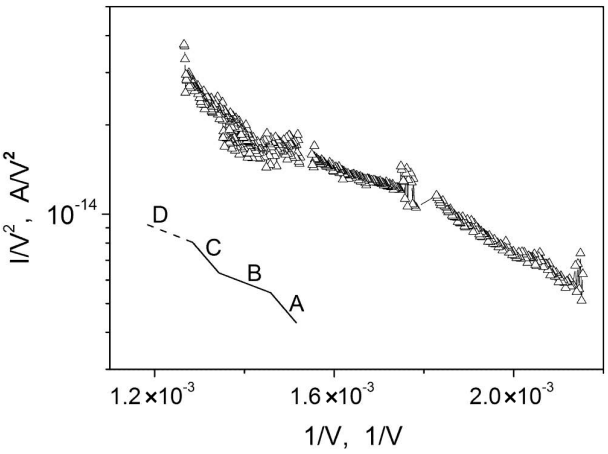

Figure 13. Fowler–Nordheim plot at field emission from AlGaN/GaN heterojunction (see Figure 8). The inset shows the different slopes in the Fowler–Nordheim plot.

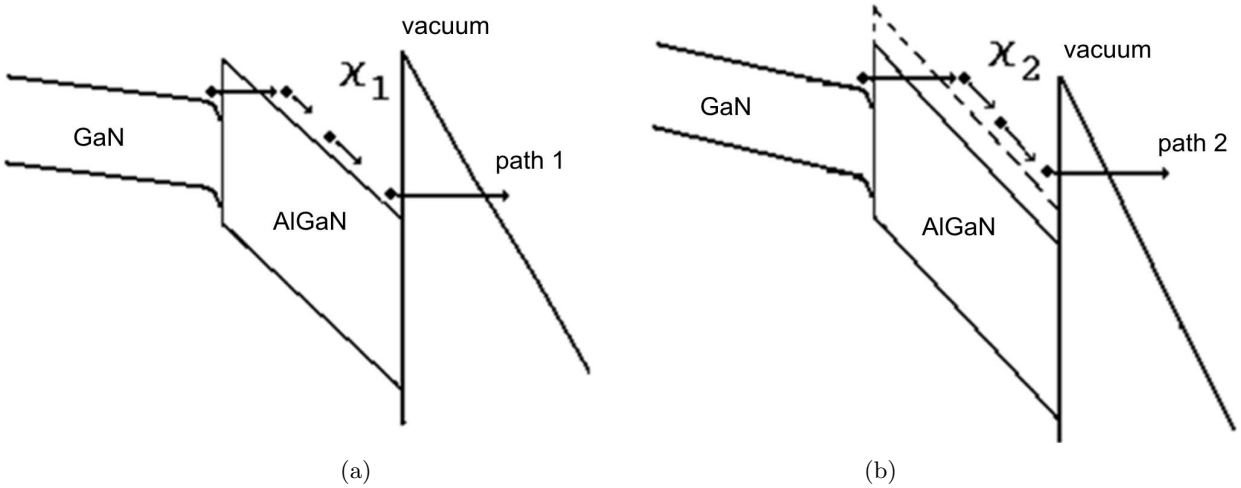

Figure 14. Energy band diagram of AlGaN on GaN with emission from AlGaN Γ-valley (a) or from AlGaN X-valley (b).

The increased slope in the FN plot (transition from B to C in Figure 13) at higher electric fields was caused by the contribution to the emission from the lower GaN tips (see Figure 8). The emission from the X-valley of AlGaN was dominated by the enhanced field emission from the Γ-valley of GaN. The electron field enhancement factor of the 2 different tips was calculated to be $\beta = 76.9$ and $\beta = 72.5$ for the AlGaN and GaN tips, respectively. The main influence on the slope change was caused by the emission material change and not by the tip shapes.

3.2.3. Field emission of ZnO nanorods

The electron field emission properties and electron transfer effect between the valleys were also investigated for ZnO field emitters (Figure 9). The FN plots of the emission current show different slopes for the small and high electric field regions (Figure 15). The model based on the electron emission from valleys having different specific electron affinities was used to explain the experimental results. Furthermore, the conduction band of nano-structured ZnO was studied with the help of these field emission experiments.

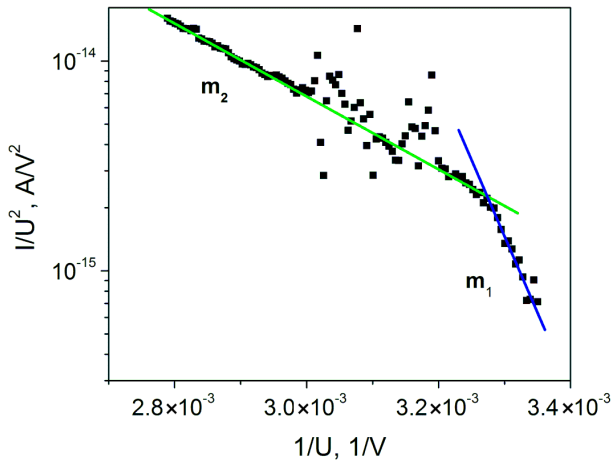

Figure 15. Fowler–Nordheim characteristic of ZnO field emitters with 2 different slopes.

At small electric fields, the emission takes place only from the lower valley, whereas at higher electric fields, the upper valley of the conduction band appears to be occupied by hot electrons and electron transfer effect takes place at the emitter tip.

The obtained value of $\chi_\Gamma / \chi_{Satellite} = 2.7$ was used to calculate $\chi_{Satellite}$ for the given value of $\chi_{\Gamma,ZnO} = 5.3$ eV. The calculated energy separation between the main and satellite valley ΔE = 3.3 eV is a little higher than the theoretically calculated value (ΔE = 3.1 eV) reported previously [68]. The effective work function from the satellite valley is much lower than that from the Γ-valley. These results can explain the usually obtained large discrepancies between extremely high field enhancement factors by fitting using the FN equation with known work function from the Γ-valley and the geometrical estimated field enhancement factors for ZnO emitters.

These functional field emitters based on ZnO materials and their ternaries can also be used as ultraviolet photodetectors and find new applications for miniaturized photofield assisted vacuum devices.

3.2.4. Functional field emitter with integrated series photoswitch

A photocathode based on semiconductor (or metal) emitters on an ultrafast photoswitch (e.g., low-temperature grown GaAs) was fabricated and used in a diode configuration (similar to Figure 4d). This configuration has the benefit of separate optimization of the field emitter tip and the photoswitch. The field emitter tips can be optimized regarding emitter radius, field enhancement factor, small turn-on voltage, high emission currents, and small beam diameter as well as chemical, physical, and thermal stability. The photoswitch in series itself should have ultrafast switching time down to subpicosecond to obtain up to THz modulated bunched electrons and low dark current to achieve high on/off ratios (Figure 16a). The position and power of the laser illumination (λ = 800 nm, P_{opt} = 20 mW) was not critical for the photomodulation. The initial configuration was achieved

with a semi-insulating GaAs photoswitch in series to the bottom of graphene nanoplatelet emitters (Figure 16b). A series connection with a low turn-on field emitter such as graphene nanoplatelets keeps the bias voltage of the complete photocathode small (e.g., ∼100 V), where the GaAs switch can modulate immediately the field emitter cathode–anode voltage from off-state (∼0 V) to on-state (e.g., ∼100 V). A low turn-on electric field of ∼1.5 V/μm (defined at 1 μA/cm^2) was obtained for this emitter. A simple low-power low-cost external green laser illumination ($\lambda \sim 532$ nm, $P_{opt} = 10$ mW) was used for triggering during field emission measurements (Figure 16b). The laser beam was focused directly onto the emitter through the quartz glass (similar to Figure 10b). Initial field emission measurements showed an on/off ratio > 200 and modulation up to 300 kHz (with nonoptimized oscilloscope measurement set-up) [69,70]. Small modification of the photocathode configuration using low-temperature grown GaAs with < 1 ps carrier lifetime and optimized measurement setup with better output coupling is necessary for short-pulse electron sources to produce fast electron bunches for promising applications as miniaturized high frequency vacuum tubes as well as THz free electron lasers [35].

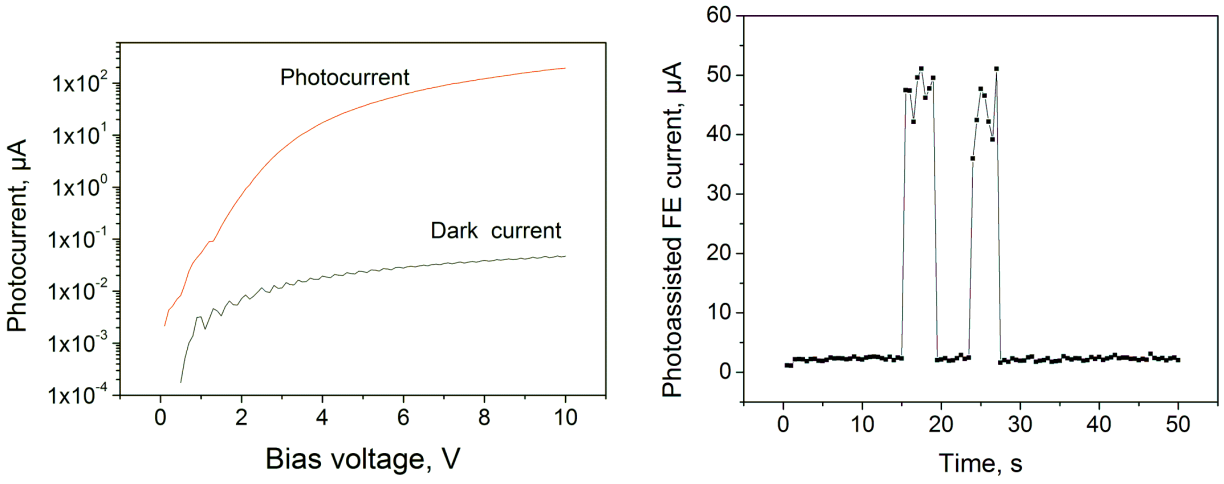

Figure 16. (a) The semi-insulating photoswitch showed low dark current and high on/off ratios using IR illumination. (b) Initial photoassisted field emission measurement using a green laser.

4. Summary

Various field emitter materials such as GaN and AlGaN were nanostructured by PEC etching, whereas ZnO field-emitter whiskers with nanometer diameter were fabricated by MOCVD growth on Si substrates. PEC etched GaN rods are promising field emitter structures due to their small tip diameter of 10–50 nm, which leads to electric field enhancement and reduced effective electron affinity. A reduced turn-on field down to E = 4 V/μm and a maximum current density of about J = 40 mA/cm^2 were obtained. Semiconductor field emitter tips showed new functionality for photoassisted field emission to generate bunched electrons directly from the emitter tip. Upon emitter illumination, the current increased immediately, which was up to one order of magnitude higher than the initial current. The photoexcited electrons contributed to the field emission process from the satellite valley due to their smaller electron affinity χ. The FN plot clearly demonstrated 2 different slopes for nonilluminated and UV illuminated emission. GaN is a compound semiconductor with multiple valleys in the conduction bands. The method based on field emission under photoillumination allowed one to determine the values of the energy difference between the Γ and the satellite valley in the conduction

band of GaN. The energy separation of the valleys was calculated as $\Delta E = 1.15$ eV, which is in good agreement with values published and much higher than in GaAs with $\Delta E = 0.31$ eV. In comparison, the calculated energy separation between the main and satellite valley of ZnO was $\Delta E = 3.3$ eV, which is a little higher than the theoretically calculated value ($\Delta E = 3.1$ eV).

The band structure reported for GaN and ZnO can be used for modulated electron field emission and be applied to the realization of miniaturized high frequency vacuum tubes as well as new functional X-ray sources with ultrashort pulses for low radiation doses. The formation of high quality GaN and ZnO NWs with controllable diameter and length and uniform distribution is still a challenging task and requires extensive experimental studies for homogeneous electron emission with high current densities.

A photocathode based on graphene nanoplatelet emitters on a semi-insulating GaAs photoswitch was fabricated and used in a diode configuration. The turn-on electric field was only $\sim$1.5 V/μm. A simple commercial laser diode triggered the field emission current with an on/off ratio $>$ 200 and a modulation frequency of 300 kHz. Using low-temperature grown GaAs with $<$ 1 ps carrier lifetime one can obtain short electron pulses for promising applications in miniaturized high frequency vacuum tubes as well as THz free electron lasers.

References

[1] Lai, R.; Mei, X. B.; Deal, W. R.; Yoshida, W.; Kim, Y. M.; Liu, P. H.; Lee, J.; Uyeda, J.; Radisic, V.; Lange, M.; et al. In *IEDM Tech. Dig.*, 2007, pp. 609–612.

[2] Graham-Rowe, D. *Nature Photonics* **2007**, *1*, 75–77.

[3] Vurgaftman, I.; Meyer, J. R.; Ram-Mohan, L. R. *Appl. Phys. Rev.* **2001**, *89*, 5815.

[4] Morkoc, B. H.; Di Carlo, A.; Cingolani, R. *Solid-State Electronics* **2002**, *46*, 157.

[5] Yilmazoglu, O.; Mutamba, K.; Pavlidis, D.; Karaduman, T. *Electron. Lett.* **2007**, *43*, 480–481.

[6] Yilmazoglu, O.; Mutamba, K.; Pavlidis, D.; Karaduman, T. *IEEE Trans. Elect. Dev.* **2008**, *55*, 1563–1567.

[7] Yilmazoglu, O.; Pavlidis, D.; Hartnagel, H. L.; Evtukh, A.; Litovchenko, V.; Semenenko, N. *J. Appl. Phys.* **2008**, *103*, 114511.

[8] Nakamura, S.; Fasol, G. *The Blue Laser Diode*; Springer: Heidelberg, Germany, 1997.

[9] Jain, S. C.; Willander, M.; Narayan, J.; van Overstraeten, R. *J. Appl. Phys.* **2000**, *87*, 965.

[10] Shealy, J. R.; Kaper, V.; Tilak, V.; Prunty, T.; Smart, J. A.; Green, B.; Eastman, L. F. *J. Phys.: Condens. Matter.* **2002**, *14*, 3499.

[11] Gelmont, B.; Kim, K.; Shur, M. *J. Appl. Phys.* **1993**, *74*, 1818.

[12] Shur, M. S.; Khan, M. A. In *GaN and related materials II (Optoelectronic properties of semiconductors and superlattices, Vol. 7)*; Manasreh, M. O.; Pearton, S. J., Eds. Gordon & Breach Science Publishers: Philadelphia, PA, USA, 2000, pp. 47–92.

[13] Crowe, T. W.; Peatman, W. C. B.; Zimmermann, R.; Zimmermann, R. *IEEE Microwave and Guided Wave Letters* **1993**, *3*, 161–163.

[14] Lin, M.-C.; Huang, K.-H.; Lu, P.-S.; Lin, P.-Y.; Jao, R. F. *J. Vac. Sci. Technol. B* **2005**, *23*, 849.

[15] Brodie, I.; Spindt, C. A. In *Advances in Electronics and Electron Physics 83*; Hawkes, P. W., Ed. Academic Press: New York, NY, USA, 1992, pp. 1–106.

[16] Yang, D.-S.; Mohammed, O. F.; Zewail, A. H. *PNAS* **2010**, *107*, 14993–14998.

[17] Nakagawa, M.; Hanawa, Y.; Sakata. T. *J. Vac. Sci. Tech. B* **2009**, *27*, 725–728.

[18] Utsumi, T. *IEEE Trans. Electron. Dev.* **1991**, *38*, 2276.

[19] Litovchenko, V.; Evtukh, A.; Kryuchenko, Yu.; Goncharuk, N.; Yilmazoglu, O.; Mutamba, K.; Hartnagel, H. L.; Pavlidis, D. *J. Appl. Phys.* **2004**, *96*, 867.

[20] Litovchenko, V. G.; Evtukh, A. A.; Yilmazoglu, O.; Mutamba, K.; Hartnagel, H. L.; Pavlidis, D. *J. Appl. Phys.* **2005**, *97*, 044911.

[21] Nemanich, R. J. In *Gallium Nitride and Related Semiconductors;* Edgar, J. H.; Strite, S.; Akasaki, I.; Amano, H.; Wetzel, C., Eds. EMIS Datareview, Series No. 23, INSPEC: London, UK, 1998, pp. 98–102.

[22] Kozawa, T.; Ohwaki, T.; Taga, Y.; Sawaki, N. In *Proc. Int. Workshop on Nitride Semiconductors*, IPAP Conf. Ser.1, 2001, pp. 989–992.

[23] Grabowski, S. P.; Schneider, M.; Nienhaus, H.; Monch, W.; Dimitrov, R.; Ambacher, O.; Stutzmann, M. *Appl. Phys. Lett.* **2001**, *78*, 2503.

[24] Yue, S. L.; Shi, C. Y.; Li, J. J.; Gu, C. Z. *J. Appl. Phys.* **2006**, *99*, 094908.

[25] Litovchenko, V. G.; Evtukh, A. A. In *Vacuum nanoelectronics. Handbook of Semiconductor Nanostructures and Nanodevices (Vol. 3), Spintronics and Nanoelectronics*; Balandin, A. A.; Wang, K. L., Eds. American Scientific Publishers: Los Angeles, CA, USA, 2006, pp. 153–234.

[26] Taniyasu, Y.; Kasu, M.; Makimoto, T. *Appl. Phys. Lett.* **2004**, *84*, 2115.

[27] Kang, D.; Zhirnov, V. V.; Sanwald, R. C.; Cuomo, J. J. *J. Vac. Sci. Technol. B* **2001**, *19*, 50.

[28] Yilmazoglu, O.; Biethan, J.-P.; Evtukh, A.; Semenenko, M.; Pavlidis, D.; Hartnagel, H. L.; Litovchenko, V. *Applied Surface Science* **2012**, *258*, 4990–4993.

[29] Litovchenko, V.; Grygoriev, A.; Evtukh, A.; Yilmazoglu, O.; Hartnagel, H. L.; Pavlidis, D. *J. Appl. Phys.* **2009**, *106*, 104511.

[30] Whaley, D. R.; Duggal, R.; Armstrong, C. M.; Bellew, C. L.; Holland, C. E.; Spindt, C. A. *IEEE Trans. Elect. Devices* **2009**, *56*, 896.

[31] Zaidman, E. G.; Kodis, M. A. *IEEE Trans. Elec. Dev.* **1991**, *38*, 2221.

[32] Whaley, D. R.; Gannon, B. M.; Smith, C. R.; Armstrong, C. M.; Spindt, C. A. *IEEE Transaction on Plasma Science* **2000**, *28*, 727–747.

[33] Choi, H. Y.; Chang, W. S.; Kim, H. S.; Park, Y. H.; Kim, J. U. *Phys. Lett. A* **2006**, *357*, 36.

[34] Jeong, J.-W.; Kang, J.-T.; Choi, S.; Kim, J.-W.; Ahn, S.; Song, Y.-H. *Appl. Phys. Lett.* **2013**, *102*, 023504.

[35] Andrews, H. L.; Brau, C. A.; Jarvis, J. D.; Guertin, C. F.; O'Donnell, A.; Durant, B.; Lowell, T. H.; Mross, M. R. *Physical Review Special Topics - Accelerators and Beams* **2009**, *12*, 080703.

[36] Bakhtyari, A.; Brownell, J. H. *Appl. Phys. Lett.* **2003**, *82*, 3150.

[37] Ganter, R.; Bakker, R.; Gough, C.; Leemann, S. C.; Paraliev, M.; Pedrozzi, M.; Le Pimpec, F.; Schlott, V.; Rivkin, L.; Wrulich, A. *PRL* **2008**, *100*, 064801.

[38] Litovchenko, V.; Evtukh, A.; Semenenko, M.; Grygoriev, A.; Yilmazoglu, O.; Hartnagel, H. L.; Sirbu, L.; Tiginyanu, I. M.; Ursaki, V.V. *Semiconductor Science and Technology* **2007**, *22*, 1092–1096.

[39] Evtukh, A.; Yilmazoglu, O.; Litovchenko, V.; Semenenko, M.; Kyriienko, O.; Hartnagel, H. L.; Pavlidis, D. *J. Vac. Sci. Technol. B* **2010**, *28*, C2A72.

[40] Evtukh, A.; Yilmazoglu, O.; Litovchenko, V.; Ievtukh, V.; Hartnagel, H. L.; Pavlidis, D. *J. Vac. Sci. Technol. B* **2012**, *30*, 022206.

[41] Shimawaki, H.; Neo, Y.; Mimura, H.; Wakaya, F.; Takai, M. In *Proc. 23rd Int. Vac. Nanoelectron. Conf.*, Palo Alto, California, USA, 2010, pp. 74–75.

[42] Caroff, P.; Dick, K. A.; Johansson, J.; Messing, M. E.; Deppert, K.; Samuelson, L. *Nature Nanotechnology* **2009**, *4*, 50–55.

[43] Huang, Y.; Duan, X.; Cui, Y.; Lieber, C. M. *Nano Letters* **2002**, *2*, 101–104.

[44] Li, Y.; Xiang, J.; Qian, F.; Gradecak, S.; Wu, S.; Yan, H.; Blom, D. A.; Lieber, C. M. *Nano Letters* **2006**, *6*, 1468–1473.

[45] Lundqvist, B. I.; Mountfield, K.; Wilkins, J. W. *Solid State Commun.* **1972**, *10*, 383.

[46] Lee, M. J. G.; Reifenberger, R. *Surf. Sci.* **1978**, *70*, 114.

[47] Yilmazoglu, O.; Pavlidis, D.; Hartnagel, H. L.; Litovchenko, V.; Evtukh, A.; Grygoriev, A.; Semenenko, N. In *IEEE Nanotechnology Materials and Devices Conference* (IEEE-NMDC2008), Kyoto, 2008.

[48] Evtukh, A.; Yilmazoglu, O.; Litovchenko, V.; Semenenko, M.; Gorbanyuk, T.; Grygoriev, A.; Hartnagel, H.; Pavlidis, D. *Phys. stat. sol. c.* **2008**, *5*, 425–430.

[49] Hartnagel, H. L.; Yilmazoglu, O.; Litovchenko, V.; Evtukh, A.; Pavlidis, D. In *Techn. Digest of 22nd International Vacuum Nanoelectronics Conference* (IVNC'09), Hamamatsu, Japan, 2009.

[50] Radon, T. *Prog. Surf. Sci.* **1998**, *59*, 331.

[51] Mutamba, K.; Yilmazoglu, O.; Sydlo, C.; Mir, M.; Hubbard, S.; Zhao, G.; Daumiller, I.; Pavlidis, D. *Superlattices and Microstructures* **2006**, *40*, 363–368.

[52] Mutamba, K., Yilmazoglu, O.; Cojocari, O.; Sydlo, C.; Pavlidis, D.; Hartnagel, H. L. In *International Semiconductor Conference* (CAS), Sinaia, Romania, vol. 1, 2006, pp. 85–92.

[53] Mutamba, K.; Yilmazoglu, O.; Sydlo, C.; Pavlidis, D.; Mir, M.; Hubbard, S.; Zhao, G.; Daumiller, I. In *Proc. Wocsdice*, Cardiff, UK, 2005, pp. 111–112.

[54] Yilmazoglu, O.; Considine, L.; Cho, E.; Pavlidis, D.; Jatta, S.; Meissner, P. In *Proc. Wocsdice* 2010, Darmstadt/Seeheim, Germany, 2010, pp. 49–50.

[55] Evtukh, A.; Yilmazoglu, O.; Litovchenko, V.; Semenenko, M.; Gorbanyuk, T.; Grygoriev, A.; Hartnagel, H.; Pavlidis, D. *Phys. stat. sol. c.* **2008**, *5*, 425–430.

[56] Wu, H.; Lin, D.; Zhang, R.; Pan, W. *J. Am. Ceram. Soc.* **2008**, *91*, 656–659.

[57] Park, W. I.; Kim, J. S.; Yi, G.-C.; Bae, M. H.; Lee, H.-J. *Appl. Phys. Lett.* **2004**, *85*, 5052.

[58] Biethan, J.-P.; Considine, L.; Pavlidis, D. *Journal of Electronic Materials* **2011**, *40*, 453–458.

[59] Biethan, J.-P.; Sirkeli, V. P.; Considine, L.; Nedeoglo, D. D.; Pavlidis, D.; Hartnagel, H. L. *Materials Science and Engineering B* **2012**, *177*, 594–599.

[60] Yilmazoglu, O.; Pavlidis, D.; Litvin, Yu. M.; Hubbard, S.; Tiginyanu, I. M.; Mutamba, K.; Hartnagel, H. L.; Litovchenko, V. G.; Evtukh, A. *Applied Surface Science* **2003**, *220*, 46–50.

[61] Yamashita, T.; Hasegawa, S.; Nishida, S.; Ishimaru, M.; Hirotsu, Y.; Asahi, H. *Appl. Phys. Lett.* **2005**, *86*, 082109.

[62] Yeo, Y. C.; Chong, T. C.; Li, M. F. *J. Appl. Phys.* **1998**, *83*, 1429.

[63] Bulutay, C.; Ridley, B. K.; Zakhleniuk, N. A. *Phys. Rev. B* **2000**, *62*, 15754.

[64] Sun, C.-K.; Huang, Y.-L.; Keller, S.; Mishra, U. K.; DenBaars, S. P. *Phys. Rev. B* **1999**, *59*, 13535.

[65] Levinshtein, M. E.; Rumyantsev, S. L.; Shur, M. S. *Properties of Advanced Semiconductor Materials: GaN, AlN, InN, BN, SiC, and SiGe*; Wiley: New York, NY, USA, 2001.

[66] Liu, Z.; Machuca, F.; Pianetta, P.; Spicer, W. E.; Pease, R. F. W. *Appl. Phys. Lett.* **2004**, *85*, 1541.

[67] Semenenko, M.; Yilmazoglu, O.; Hartnagel, H. L.; Pavlidis, D. *J. Appl. Phys.* **2011**, *109*, 023703.

[68] Fan, W. J.; Xia, J. B.; Agus, P. A.; Tan, S. T.; Yu, S. F.; Sun, X. W. *J. Appl. Phys.* **2006**, *99*, 013702.

[69] Yilmazoglu, O.; Al-Daffaie, S.; Nick, C.; Joshi, R.; Yadav, S.; Hartnagel, H. L.; Schneider, J. J.; Thielemann, C. In *25th International Vacuum Nanoelectronics Conference (IVNC 2012)*, Jeju, South Korea, 2012.

[70] Yilmazoglu, O.; Al-Daffaie, S.; Küppers, F.; Hartnagel, H. L.; Neo, Y.; Mimura, H. In *27th International Vacuum Nanoelectronics Conference (IVNC 2014)*, Engelberg, Switzerland, 2014.